NANO LETTERS

Letter

pubs.acs.org/NanoLett

Two Color DNA Barcode Detection in Photoluminescence Suppressed Silicon Nitride Nanopores

Ossama N. Assad,[†] Nicolas Di Fiori,[†] Allison H. Squires,[†] and Amit Meller*[,†,‡]

[†]Department of Biomedical Engineering, Boston University, Boston, Massachusetts 02215 United States

[‡]Department of Biomedical Engineering, Technion − Israel Institute of Technology, Haifa, Israel 32000

Supporting Information

ABSTRACT: Optical sensing of solid-state nanopores is a relatively new approach that can enable high-throughput, multicolor readout from a collection of nanopores. It is therefore highly attractive for applications such as nanopore-based DNA sequencing and genotyping using DNA barcodes. However, to date optical readout has been plagued by the need to achieve sufficiently high signal-to-noise ratio (SNR) for single fluorophore sensing, while still maintaining millisecond resolution. One of the main factors degrading the optical SNR in solid-state nanopores is the high photoluminescence (PL) background emanating from the silicon nitride (SiN_x) membrane in which pores are commonly fabricated. Focusing on the optical properties of SiN_x nanopores we show that the local membrane PL intensity is substantially reduced, and its spectrum is shifted toward shorter wavelengths with increasing e-beam dose. This phenomenon, which is correlated with a marked photocurrent enhancement in these nanopores, is utilized to perform for the first time single molecule fluorescence detection using both green and red laser excitations. Specifically, the reduction in PL and the concurrent measurement of the nanopore photocurrent enhancement allow us to maximize the background suppression and to detect a dual color, five-unit DNA barcode with high SNR levels.

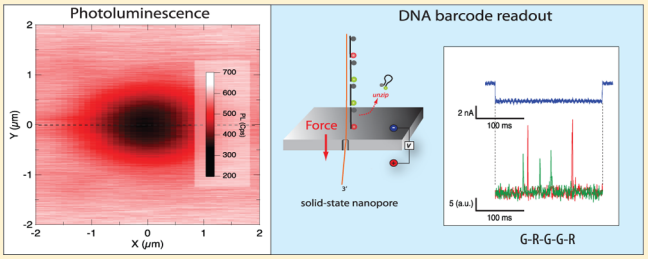

KEYWORDS: *Solid-state nanopore, silicon nitride, optical detection, photoluminescence, electron-beam, single-molecule*

Solid-state nanopores offer immense potential as single-molecule sensors for biomedical applications,[1−4] particularly nucleic acid sequencing[5] and protein characterization.[6−8] Typically, the method involves a measurement of the ion current flowing through a single nanopore during the electrically driven passage of a charged biomolecule. Optical sensing of nanopores is a relatively new approach that can enable high-throughput, multicolor and multiplexed readout from a collection of nanopores, while circumventing the microfluidics and complex integrated circuitry required for multichannel electrical recording from an array of nanopores.[9−13] Optical sensing is therefore highly attractive for applications such as DNA sequencing and DNA barcoding of specific genes. However, optical readout with sufficiently high signal-to-noise ratio (SNR) and millisecond resolution for individual fluorophores has been challenging, especially when using blue-green excitations. Recent studies employing background-suppression methods, such as total internal reflection (TIR), enabled the detection of single fluorophores in solid-state nanopores, but these studies were limited to fluorophores with long wavelength excitation and emission (λ > 640 nm),[10] which severely restricted the available set of compatible high brightness fluorophores.

The main contribution to degradation of the optical SNR in solid-state nanopores is laser-induced photoluminescence (PL) from the silicon nitride (SiN_x) membrane surrounding the nanopores. PL in supported SiN_x films is a well-characterized phenomenon,[14−19] however much less is known about the PL in free-standing, ultrathin (<100 nm) SiN_x membranes immersed in aqueous salt buffers, such as those with which nanopore experiments are conducted. Previous approaches to reduce background of solid state nanopores have included sophisticated fabrication techniques to directly block emission from areas away from the nanopore[20] as well as coating the SiN_x membrane with materials emitting low photoluminescence, such as titanium dioxide.[21] Sawafta and co-workers recently achieved some reduction of the native SiN_x background using He^+ ion bombardment, but this method did not permit single-fluorophore sensing.[22] Most importantly, until now optical SNR in nanopores has not been reduced to a level permitting single-fluorophore sensing in the green-yellow spectral range, where the majority of high quantum-yield (and high brightness) fluorophores are available for single-molecule imaging.[23]

We recently reported that exposure of SiN_x membranes to a focused e-beam can produce highly photoreactive nanopores, which can be reversibly charged using low-power green laser light.[24] This optoelectrical phenomenon induces an electro-

Received: November 20, 2014
Revised: December 16, 2014
Published: December 19, 2014

   dx.doi.org/10.1021/nl504459c | *Nano Lett.* 2015, 15, 745−752

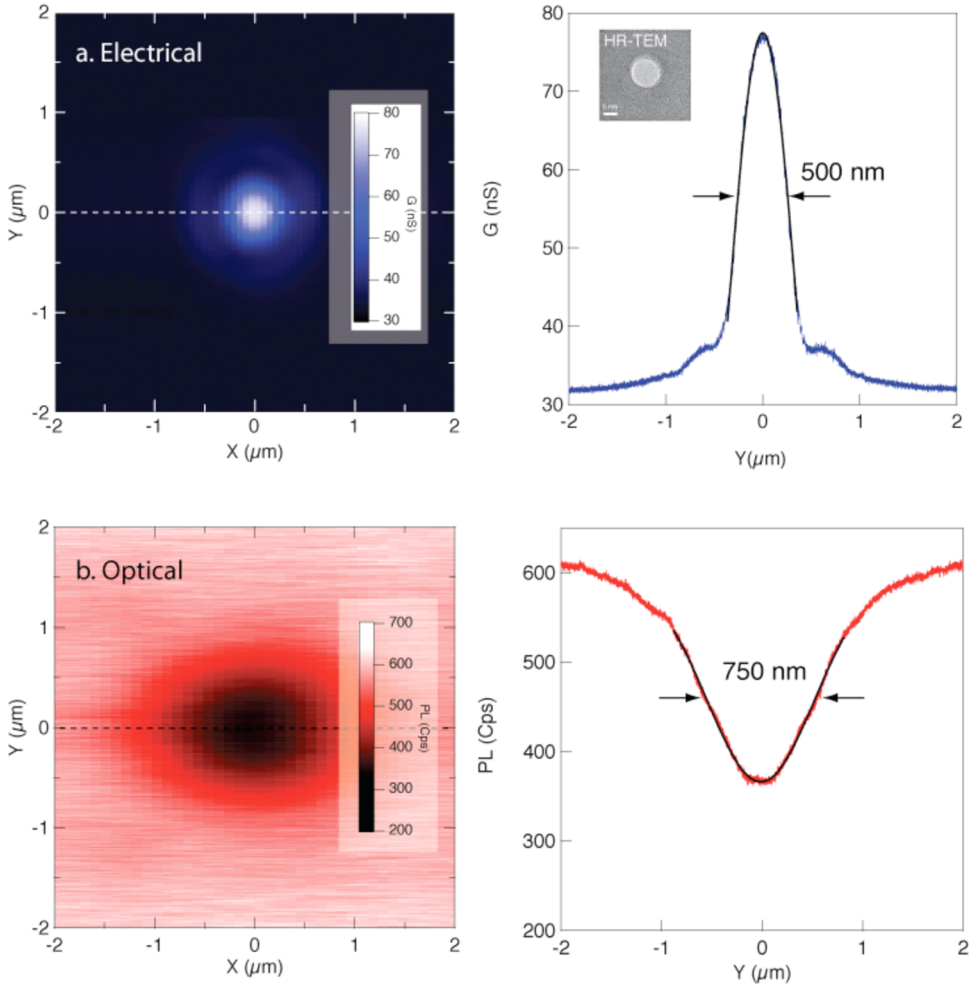

Figure 1. Simultaneous electrical and optical signals from a 4 × 4 μm scan of SiN_x in which a 10 nm diameter nanopore was drilled (see inset for HR-TEM image). Upper panel: Ion conductance map during scan showing more than 2-fold increase in current due to the opto-electrical effect when the laser spot (λ = 532 nm) is fully aligned with the pore. Lower panel: photoluminescence emission map from the SiN_x membrane showing a 2-fold decrease in intensity around the pore region. The right-hand panels display line profiles through the intensity maps (at the locations indicated by dotted lines at left). Black lines represent Gaussian fits to estimate the effective width of the profiles.

osmotic flow through the nanopore, which in turn was utilized to regulate the translocation speed of analytes such as DNA and proteins. This effect was attributed to preferential depletion of nitride atoms over silicon during the e-beam drilling process, creating a local silicon-rich damaged area at the location of e-beam irradiation.[25] Here we focus on the impact of controlled focused e-beam radiation on the optical properties of nanopores made in SiN_x membranes. Specifically, we present here evidence of local and tunable reduction of membrane PL emission induced by irradiation with a focused electron beam. We have spectrally characterized this reduction in PL as a function of e-beam dose and observed a consistent shift in the SiN_x emission spectrum with increasing e-beam exposure. This reduction in PL is not restricted to the exposed area but extends over a local area (several hundred nanometers) around the pore, suggesting that it may be related to thermally induced changes in the membrane material structure during e-beam exposure. Notably, the reduction in the PL emission enables us to substantially improve SNR to the point where we can record for the first time simultaneous electrical and optical translocations of singly labeled DNA barcodes in the both green-yellow fluorophore (λ_{peak} = 565 nm) and red fluorophores (λ_{peak} = 665 nm) using single photon counters in a confocal optical nanopore microscope.

High-resolution aberration corrected TEM (Titan 80-300 FEG-S/TEM, FEI) was used to fabricate single nanopores in Low Pressure Chemical Vapor Deposition (LPCVD) low-stress SiN_x membranes. Except where otherwise stated, membranes consisted of 60 nm thick freestanding windows of SiN_x approximately 20 × 20 μm^2 in size. These membranes were subsequently thinned down using a controlled reactive ion etching (RIE) process applied to ~1.5 μm diameter wells, leading to 15 nm thick regions where pores were drilled (see Supporting Information). Piranha-cleaned solid-state nanopores were freshly assembled in a custom-made Teflon cell permitting low-noise electrical measurements and direct imaging using a high-magnification microscope objective. The chips were immersed in electrolyte solution consisting of a salt (1 M KCl) buffer in both chambers (cis and trans). Collimated laser beams (488, 532, or 640 nm) were focused at the nanopore area through the microscope objective lens, forming a diffraction-limited spot for confocal illumination. Light was collected by the same objective and imaged onto (i) three spectrally separated avalanche photodiodes (APDs) for photon counting (confocal), or (ii) a spectrophotometer for measuring

dx.doi.org/10.1021/nl504459c | Nano Lett. 2015, 15, 745−752

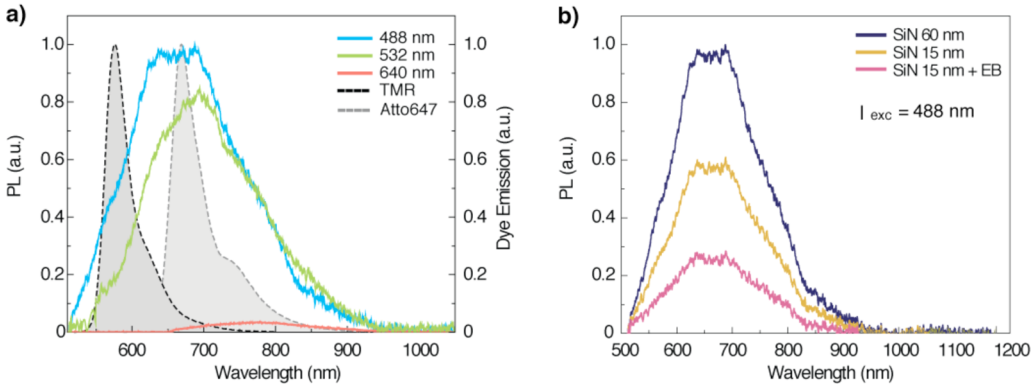

Figure 2. Photoluminescence spectra of thin SiN_x membranes suspended in aqueous solutions. (a) The spectra obtained using either blue (488 nm), green (532 nm), or red (640 nm) lasers. Data is normalized by the incoming lasers intensities to permit comparison. The emission spectra of two common single-molecule fluorophores TMR and Atto647 are shown for reference (black and gray dashed lines, respectively). (b) Spectra obtained from three regions on the SiN_x membrane excited by 488 nm laser: (1) 60 nm thick (dark blue), (2) 15 nm thick (orange), and (3) 15 nm thick exposed to high electron beam radiation (magenta). All samples displayed an emission band from 550 to 850 nm with a peak around 650 nm.

the emitted photons as a function of wavelength. The ion current flowing through the pore was measured using two Ag/AgCl electrodes immersed in the *cis* and the *trans* chambers, respectively, connected to an Axon Axopatch 200B patch-clamp amplifier and digitized at 250 kS/s (16 bits) with a National Instruments (NI-6211) card. The digital signal representing the photon emission was recorded by a counter board (NI-6602) utilizing hardware synchronization between the ion current and the photons counts. Detailed descriptions of our setups are provided in the Supporting Information.

Figure 1 displays a synchronous recording of the PL emission from a silicon nitride membrane and the ionic current flowing through the pore at a fixed voltage level while a nanopositioner scanned a 4 × 4 μm^2 region of the membrane using a 10 mW focused laser beam (532 nm). As previously reported, when the laser spot overlapped with the nanopore location we observed an increase in the ionic current with maximum magnitude nearly twice that of the original current. This photoconductive effect was evident even when using laser powers of just a few milliwatts.[24] We illustrate this effect in Figure 1: The upper panel shows an intensity surface plot of the ionic current flowing through this pore as a function of laser spot position (left upper panel). A line scan through the center of the image shows a clear symmetric peak in the ion current with a FWHM of 500 nm (right upper panel). The inset shows a TEM image of the 10 nm pore used in this test.

Strikingly, the simultaneous acquisition of PL emanating from the SiN_x membrane during the surface scan reveals a pronounced reduction in PL emission concentric with the area that showed current enhancement (Figure 1b). Analysis of the spatial distributions of the ionic flow and PL profiles (right-hand panels) reveals that while the former is limited by the laser point spread function (PSF, FWHM =500 nm), the PL reduction effect extends beyond it (FWHM >750 nm). This suggests that the effect of the e-beam on the SiN_x extends substantially beyond its local "probe size" (typically <1 nm for HR-TEM), possibly by inducing heating and local diffusion of atoms.[26]

We first characterized the optical properties of the suppressed PL emission by measuring its spectra under three laser excitations (488, 532, and 640 nm). In each case, the membrane *z*-plane was carefully aligned with the laser spot center by means of a nanopositioner, and emission intensities were scaled according to the incoming laser intensity to ensure proper normalizations. The spectra were obtained by coupling a spectrometer (Ocean Optics, USB4000) to our system as shown in the Supporting Information. Our results (Figure 2a) indicate that (i) the blue and green excitations both produce a broad PL emission band (roughly 550−850 nm) with maximum emission around 650−700 nm and (ii) the spectra from the red excitation is substantially reduced as compared to the spectra for blue or green excitation. Notably, the PL emission spectra when exciting with green and blue lasers overlap substantially with the emission spectra of many of the common high brightness fluorophores spanning the green to far-red range. As a reference, the emission spectra of two common high brightness fluorophores, tetramethylrhodamine (TMR, black curve) and Atto647 (gray curve) are overlaid in Figure 2a. This measurement explains why single fluorophore detection has not previously been reported in solid-state nanopores using blue-green laser excitations. Instead, previous studies have been restricted to the use of red laser excitation and far-red dyes.[10]

We next measured the PL spectrum emitted from the following three different regions of the same silicon nitride membrane: (i) a region 60 nm thick, (ii) 15 nm thick (thinned-down area), and (iii) 15 nm thickness after exposure to a high e-beam dose, forming a nanopore. Figure 2b shows the spectra obtained under excitation by a 488 nm laser (similar measurements obtained with the two other lasers are shown in the Supporting Information). The following three important features can be observed: (i) the shapes of the three spectra for these three regions are similar, (ii) thinning down the silicon nitride from 60 to 15 nm leads to reduction of the PL intensity, and (iii) exposure of the 15 nm thick area to the electron beam results in an additional reduction by a factor of 2 with respect to the unexposed 15 nm thick area.

A similar trend can be seen from the more quantitative measurements shown in Figure 3. The emission spectra (Figure 2b) were used as a guide to spectrally split the PL emission using dichroic mirrors into the following three bands: (I) 500−650 nm, (II) 650−750 nm, and (III) 750−900 nm. The photons emitted in each of these bands were probed using three avalanche photodiodes (APDs). To restrict the emission volume, emitted light from the membrane was first focused onto a 25 μm pinhole defining a narrow region centered around

dx.doi.org/10.1021/nl504459c | *Nano Lett.* 2015, 15, 745−752

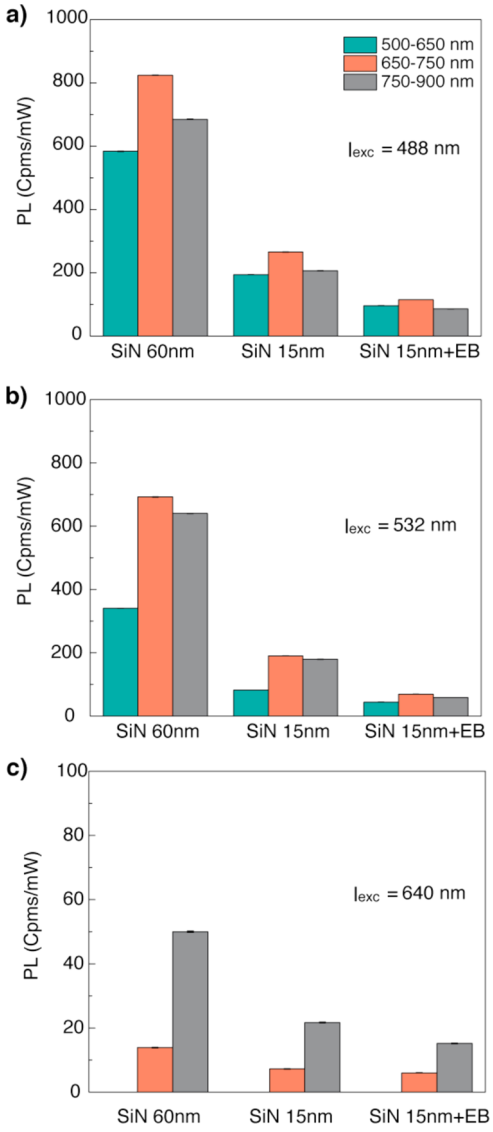

Figure 3. Confocal measurements of photocounts emitted from three regions on the SiN_x membranes, 60 nm thick, 15 nm thick, and 15 nm thick, exposed to high electron beam, measured at the following three wavelength bands: (I) 500−650 nm (green), (II) 650−750 nm (red), and (III) 750−900 nm (gray). The three panels correspond to three different laser excitations (a) 488 nm, (b) 532 nm, and (c) 640 nm.

the pore's location (roughly one wavelength FWHM). As before, we normalized the results by the corresponding incoming laser powers to maintain consistency among the different laser excitations. First, we observe that irrespective of the excitation wavelength, thinning down a region of the membrane and further exposing it to the e-beam significantly reduces the PL in the visible range: seven-fold for blue and green excitation and four times for red. Second, consistent with the results in Figure 2a, longer excitation wavelengths produce weaker PL intensities, albeit weaker reduction (note the different *Y*-scale in Figure 3a−c). Specifically, illumination of the SiN_x membrane with the red laser shows a 10-fold decrease in photon count as compared with the other two. Interestingly, the Stokes shift seems to be roughly 200 nm for all measurements.

To determine the effect of e-beam exposure on PL intensity and spectra, a study was performed to compare areas of the same membrane, which had been irradiated with varying e-beam doses. To facilitate the localization of these exposed regions on the membrane we fabricated a 3 × 3 array of circular RIE-thinned regions, each ∼1.5 μm in diameter and 15 nm thick (Figure 4a inset). Six of these were exposed to a series of increasing electron beam dosages at their centers. These thinned regions were visually distinguishable from the rest of the membrane under white-light illumination. Figure 4a displays the normalized PL intensity from a 488 nm laser excitation as a function of the e-beam dose. The PL intensity dropped from an initial level of 670 ± 30 counts per millisecond per milliwatt (Cpms/mW) with no e-beam dose to less than 330 ± 14 (Cpms/mW) when the e-beam dose reached 56×10^6 (electron/nm^2), yet remained roughly at that level for even larger e-beam dosages. This data could be well fit by an exponential function with an offset baseline of 270 ± 20 (Cpms/mW). The fact that the dose curve does not decay asymptotically to zero indicates that there are at least two contributions to the SiN_x PL, one that is directly affected by e-beam irradiation and a baseline level that is unaffected by the e-beam. In a subsequent study, we irradiated two SiN_x membranes, 60 and 15 nm thick, with the e-beam for an extended period of time (see Figure S4 in the Supporting Information) and found that both reach similar baseline levels after prolonged radiation. One possible explanation for this observation is that this PL contribution arises from the SiN_x−water interfaces (oxidized surfaces) and not from the bulk material.[27,28]

We further analyzed the effect of e-beam dosage on the membrane's spectral properties by measuring the relative contribution in each of the three APD channels for each dose level (Figure 4b). As can be seen from the figure, the red and far-red contributions of the PL (red and gray markers, respectively) showed only a mild decrease with dose. On the other hand, the green contribution (green markers) displayed a marked increase with e-beam dose, showing a shift of PL toward higher energies. While the source of this mild blue-shift in the SiN_x PL after e-beam illumination requires further investigation (for example, by utilizing focused high-resolution material composition in advanced electron microscopy), we note that the spectral shift we observe in these measurements is clear and consistent, and as explained below can be utilized to explore its relationship with the light-induced charging phenomena.

Figures 3 and 4 suggest that highly localized e-beam irradiation of SiN_x during the drilling process of solid-state nanopores induces substantial alterations to the membrane's material properties, resulting in a measurable reduction of the PL intensity and a blue shift of its spectrum. In Figure 1, we showed the effect of visible light on the ionic current, which we termed the "photo-conductive effect". Now we are in position to evaluate the relationship between PL suppression and the photoconductive enhancement in solid-state nanopores, as these two effects are important for enhancing the resolution of both electrical and optical based nanopore sensing. To this end we drilled two sets of nanopores on identically prepared SiN_x membranes. We used a small e-beam dose for the first set and roughly a 9-fold larger dose for the second set. These pores were assembled on our confocal nanopore microscope where we simultaneously measured the photoreactivity of each pore along with the local PL emissions. Figure 5a shows open pore currents as a function of the laser intensity used to evaluate the nanopores' photoreactivity coefficient γ, calculated as in Di

dx.doi.org/10.1021/nl504459c | *Nano Lett.* 2015, 15, 745−752

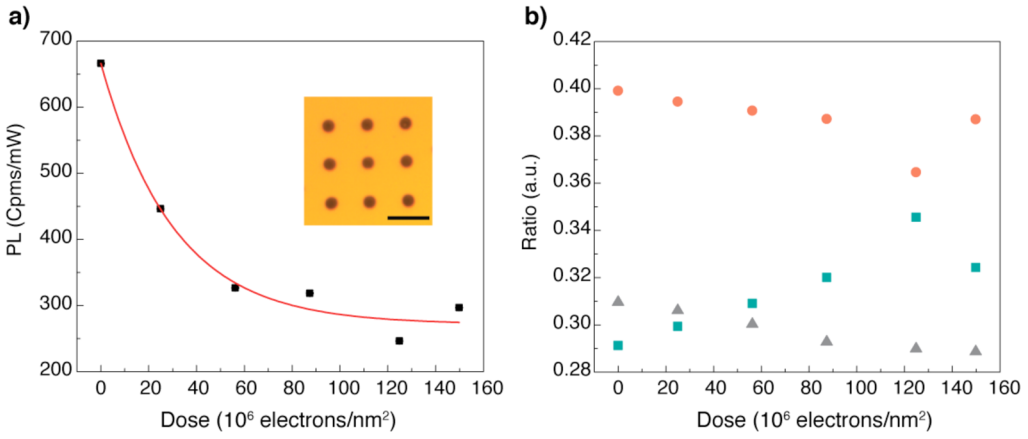

Figure 4. (a) Dependence of TEM electron beam dosage on the total PL count (measured using λ = 488 nm). The red line is an exponential fit to the data points. Inset: bright-field optical image showing the array of locally thinned down SiN_x wells (roughly 1.5 μm diameter) that were exposed to a various electron beam dosage, scale bar is 5 μm. (b) The fraction of PL in the different channels, normalized to the total PL, as a function of the e-beam dosage: 500−650 nm (squares), 650−750 nm (circles), and 750−900 nm (triangles).

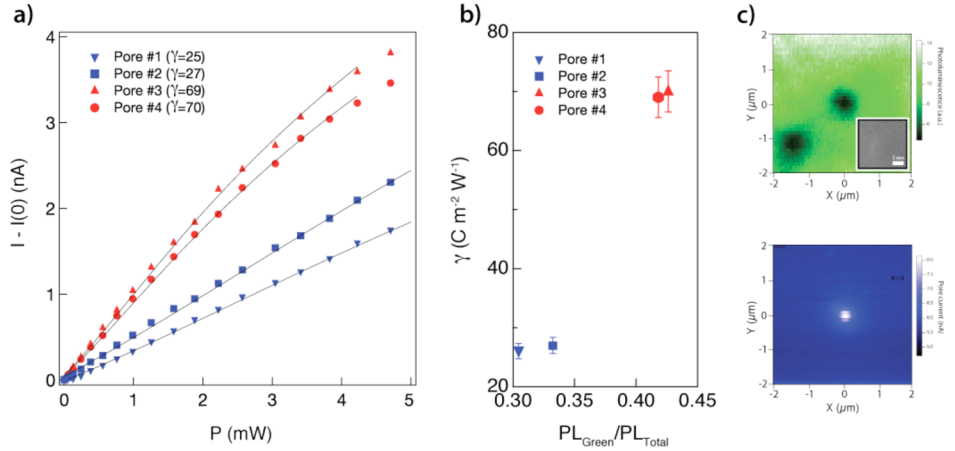

Figure 5. Correlation between the nanopores photoreactivity and magnitude of PL suppression. (a) Measurements of the photoreactivity parameter γ for four nanopores of similar diameter (4 ± 0.5 nm) but drilled using two different e-beam dosages: 60 and 500 s exposure times (blue and red markers, respectively). The change in open pore currents as a function of laser intensity at constant voltage (V = 300 mV) is fit to eq 2 in Di Fiori et al.[24] (black lines) to obtain γ. (b) Photoreactivity γ as a function of the fraction of PL in the green channel (500−650 nm) over total PL (500−900 nm) for the same four nanopores. The amount of e-beam exposure determines the final photoreactivity and PL emission spectra of the pores. All pores were drilled consecutively in identical membranes. (c) An area of the SiN_x membrane in which a nanopore is fabricated at its center and another point is exposed to the e-beam with no pore. PL scan (top) shows similar magnitude of suppression at the two locations, while ion conductance map (bottom) shows a 2-fold increase only at the pore location in the center of the image. Inset shows TEM image of the pore (~5 nm).

Fiori et al.[24] Consistent with previous studies, the pores drilled using a small e-beam dosage produced more than 2-fold smaller γ values (26 ± 2 C/m^{2}W) than the pores drilled using larger dosage (70 ± 3 C/m^{2}W). Interestingly and consistent with Figure 4b, the high dosage pores showed a marked blue shift as compared with the low e-beam dose drilled pores (Figure 5b), indicating that the nanopores photoreactivity and magnitude of PL suppression phenomena in nanopores are linked.

Furthermore, we note that the local reduction of PL under e-beam irradiation of SiN_x membranes does not require creation of a nanopore or any similar perforation of the membrane with the e-beam. In Figure 5c, we show simultaneous optical (top) and electrical (bottom) signals from a 4 × 4 μm^2 scan of a SiN_x membrane in which a single 5 nm diameter nanopore was fabricated at the center of the scanned area (see inset for HR-TEM image), and a second nearby spot was exposed to the e-beam without forming a pore. The ion conductance map shows almost a 2-fold increase in current during scan when the 532 nm laser spot is aligned with the pore. In contrast, the photoluminescence emission map from the membrane shows a 2-fold decrease in intensity in both regions that were exposed to e-beam.

The improved PL properties of the e-beam irradiated SiN_x translate directly to superior SNR of fluorescence measurements in solid-state nanopores in a broad spectral range. Moreover, the correlation of PL suppression with the photoreactivity phenomenon, as illustrated in Figure 5, can be also utilized to align the nanopore in the $x-y-z$ directions with the pinhole with subwavelength resolution, thus permitting maximal confocal background suppression. To illustrate the applicability of our findings to single-molecule optical detection we used a custom designed DNA barcode constructs (Figure 6a,d) consisting of five 16-nucleotide long molecular beacons hybridized in head-to-tail configuration

dx.doi.org/10.1021/nl504459c | Nano Lett. 2015, 15, 745−752

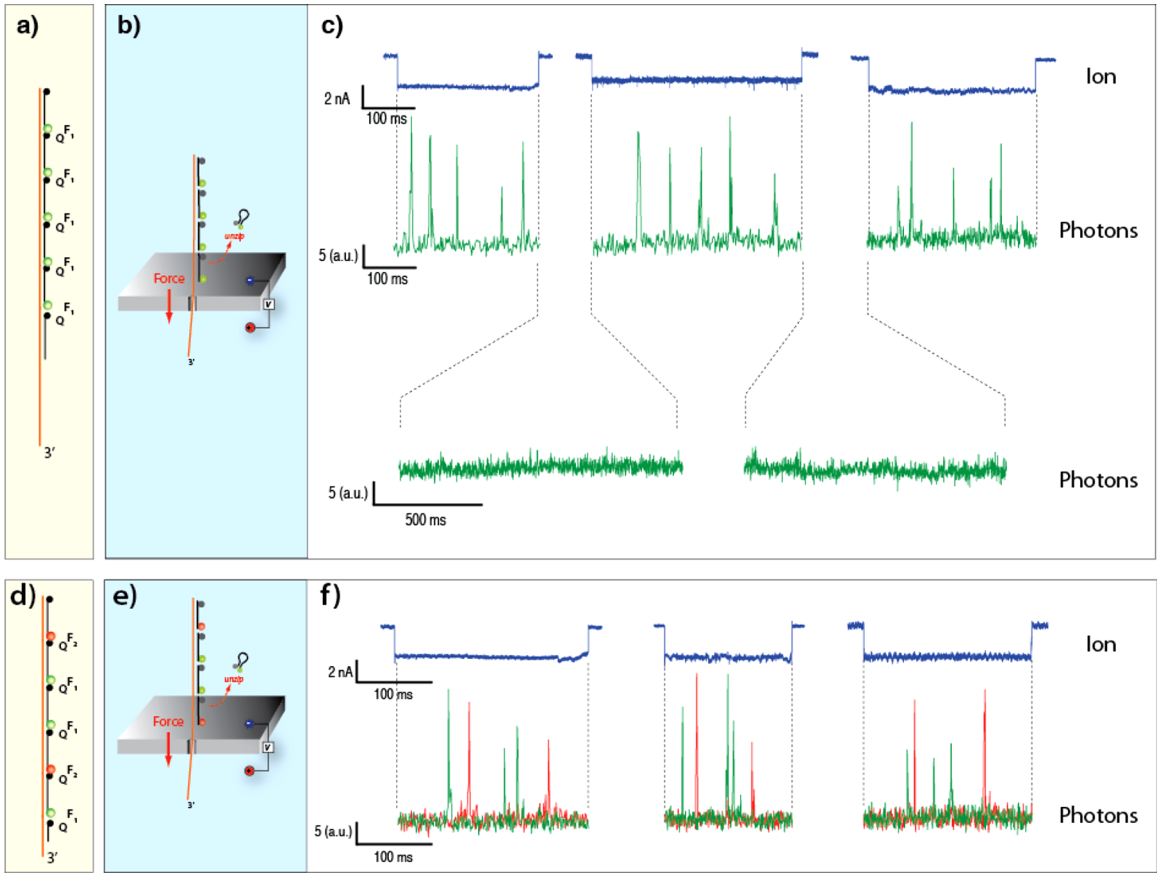

Figure 6. High SNR measurements of one- and two-colors single fluorophores DNA barcodes in the green and red channels. (a,d) Single-stranded DNA template harboring 16-mer binding sequences for five molecular beacons labeled with either green ("F_1") fluorophores (a) or a unique sequence of green and red ("F_1" and "F_2", respectively) fluorophores (d), as well as a quencher oligo were constructed. (b,e) A schematic illustration of the nanopore beacons unzipping setup. (c,f) Typical unzipping events using a low photoluminescence 3 nm pore, where optical and electrical signals are measured simultaneously, showing five clear photon bursts per event, in the green channel (c) or green and red channels (f) according to the DNA templates. The optical signal to background ratio is greater than 10 in most cases. Optical traces recorded during the open pore periods as defined by the ion currents (lower panel in c) showed no optical photon bursts.

along template strand (orange lines) such that each fluorophore was placed next to a broad-range quencher molecule (BHQ-2), in a similar design to that used by McNally et al.[10] Two different DNA templates were made: a five unit single color construct harboring sites for 5-carboxytetramethylrhodamine (TMR) labeled beacons, or a five unit dual-color construct harboring sites for TMR and Atto647 labeled beacons. In addition, a leading quencher-only oligonucleotide was hybridized to quench the first fluorophore. Full DNA sequences of these molecules are provided in the Supporting Information. On the basis of previous experiments,[10] when the molecular beacons are unzipped from the single-stranded DNA, we expect to observe the emission of well-defined photon bursts. Moreover, as previously reported the time delay between single-molecule unzipping events is a stochastic process obeying a well-defined Poisson distribution that depends on the duplex sequence, applied voltage, nanopore diameter, and temperature.[10,29] Using ~3 nm diameter low PL nanopores we recorded the electrical and optical signals (green and red APD channels) simultaneously while exciting fluorophores using the 532 and 640 nm lasers. The electrical blockade traces, recorded synchronously with the optical signals, ensure that the optical bursts are obtained only when a DNA strand is inserted in the nanopore, thus circumventing an erroneous identification of random photon bursts from DNA molecules that diffuse in the nanopore vicinity without entering the pore. Figure 6c displays three single-color events. During the time that the DNA is translocating through the pore (indicated independently by the electrical current change), we observe five discrete photon bursts, associated with the unzipping and fast diffusion of the five molecular beacons hybridized to our DNA molecule. As expected, photon bursts were only observed during pore blockades; no photon bursts were recorded in the time between events as shown in the lower panel of Figure 6c.

A similar experiment using dual-color DNA template is shown in Figure 6f. As before the electrical signal, recorded simultaneously with the optical signals, ensures that the optical traces overlap with the translocation of DNA molecules through the pore. Consistent with the designed DNA template (See Supporting Information) we observe a sequence of green/red photon bursts, which reveal its unique barcode and matches perfectly its design (Figure 6d). Notably, in both the single and the two color examples we obtain a relatively high SNR (amplitude of the fluorescence spike over the rms of the background) in the range of 3−10. We attribute this to two main factors. First, the overall low PL emission achieved by the extensive e-beam exposure. Second, utilization of the photoconductive effect in these pores to align the nanopore with the confocal pinhole, thus achieving a maximal background rejection.

dx.doi.org/10.1021/nl504459c | Nano Lett. 2015, 15, 745−752

Nanopore drilling is achieved through a combination of radiolysis due to inelastic scattering (heating, ionization, X-ray generation, Auger electron generation) and knock-on effects from elastic scattering (creation of point defects, sputtering),[25,30] and must impart enough energy to fluidize the membrane and permit-controlled shrinking of nanopores.[26,31−33] Previous studies suggest that possible sources of PL in SiN_x include at least two possible mechanisms, namely, band tail effects and silicon nanocrystals.[17,34] Band tail luminescence results from forced radiative recombinations of neighboring excited carriers with spectral properties determined by the local band structure.[35] Silicon nanocrystals are formed during deposition and/or annealing.[14,19,36,37] Both explanations suggest that PL is dependent upon silicon content and sample heating.[38] The decrease in PL that we observe and the spatial extent of this decrease may be related to the enriched silicon content of the membrane and to the inelastic heating during e-beam irradiation. Detailed analysis of local material properties will be needed to fully describe the underlying mechanism of PL suppression that we observe.

We previously reported that e-beam irradiation affects the photoreactivity properties of the SiN_x membranes, allowing visible light to reversibly induce surface charges. Here, we characterized the related optical PL properties of the nanopore system and found that the background photoluminescence of SiN_x membranes may be substantially reduced by e-beam irradiation to allow single-molecule fluorescence detection in a broad spectral range. This reduction is evident primarily under blue or green laser excitations, which previously were not viable options for single-fluorophore sensing in nanopores due to poor SNR. The correlation of the PL suppression with the photoconductive enhancement (Figure 5) allows us to align our nanopore with the excitation/emission system with subwavelength precision, permitting near-optimal background rejection in the confocal microscope. The synergistic effects of PL reduction and confocal background suppression allow us for the first time to use green laser excitation and detect orange and red fluorophores marking a dual color DNA barcode molecule. Further studies, and perhaps detailed elemental analysis of the e-beam affected zone, will be needed to pinpoint the exact compositional or morphological alterations of the SiN_x during e-beam exposure. However, the results presented here offer a highly practical technique to rapidly and reproducibly control the photoreactivity and photoluminescence of SiN_x nanostructures, enlarging the set of fluorophores that are compatible with optical single-molecule nanopore sensing and directly impacting emerging applications including nanopore-based DNA sequencing.

■ ASSOCIATED CONTENT

Supporting Information

Nanochips and nanopore fabrication methods, chips cleaning and assembly procedures, detailed design of the simultaneous confocal and electrical nanopore setup, additional photoluminescence spectra of the SiN_x membrane, correlation between the photoluminescence reduction and e-beam dosage or membrane thickness, details of the photoreactivity measurements of Figure 5, and the oligonucleotides sequences used in this study. This material is available free of charge via the Internet at http://pubs.acs.org.

■ AUTHOR INFORMATION

Corresponding Author

*E-mail: ameller@bu.edu.

Author Contributions

O.N.A and N.D.F contributed equally.

Notes

The authors declare no competing financial interest.

■ ACKNOWLEDGMENTS

We acknowledge Tal Gilboa and Daniel Bar for kind assistance in data analysis and nanopore fabrication. Financial support from the National Institutes of Health (NHGRI Grant R01 HG-005871), from the Marie Curie People award (GA-2010-277060, ERC), and from the Israeli Centers of Research Excellence (I-CORE) program (Center #1902/12) are acknowledged. The authors also thank the staff at the Harvard University Center for Nanoscale Sciences (CNS) and the Technion Electron Microscopy Center for dedicated support.

■ REFERENCES

(1) Stoloff, D. H.; Wanunu, M. *Curr. Opin. Biotechnol.* **2013**, *24* (4), 699−704.

(2) Meller, A. Nanopores: Single-Molecule Sensors of Nucleic Acid-based Complexes. In *Advances in Chemical Physics*; Rice, S. A., Dinner, A. R., Eds.; Wiley: New York, 2012; Vol. *149*.

(3) Venkatesan, B. M.; Bashir, R. *Nat. Nanotechnol.* **2011**, *6* (10), 615−624.

(4) Dekker, C. *Nat. Nanotechnol.* **2007**, *2* (4), 209−215.

(5) Branton, D.; Deamer, D. W.; Marziali, A.; Bayley, H.; Benner, S. A.; Butler, T.; Di Ventra, M.; Garaj, S.; Hibbs, A.; Huang, X.; Jovanovich, S. B.; Krstic, P. S.; Lindsay, S.; Ling, X. S.; Mastrangelo, C. H.; Meller, A.; Oliver, J. S.; Pershin, Y. V.; Ramsey, J. M.; Riehn, R.; Soni, G. V.; Tabard-Cossa, V.; Wanunu, M.; Wiggin, M.; Schloss, J. A. *Nat. Biotechnol.* **2008**, *26* (10), 1146−1153.

(6) Firnkes, M.; Pedone, D.; Knezevic, J.; Döblinger, M.; Rant, U. *Nano Lett.* **2010**, *10* (6), 2162−2167.

(7) Yusko, E. C.; Johnson, J. M.; Majd, S.; Prangkio, P.; Rollings, R. C.; Li, J.; Yang, J.; Mayer, M. *Nat. Nanotechnol.* **2011**, *6* (4), 253−260.

(8) Larkin, J.; Henley, R. Y.; Muthukumar, M.; Rosenstein, Jacob K.; Wanunu, M. *Biophys. J.* **2014**, *106* (3), 696−704.

(9) Soni, V. G.; Singer, A.; Yu, Z.; Sun, Y.; McNally, B.; Meller, A. *Rev. Sci. Instrum.* **2010**, *81* (1), 014301−7.

(10) McNally, B.; Singer, A.; Yu, Z.; Sun, Y.; Weng, Z.; Meller, A. *Nano Lett.* **2010**, *10* (6), 2237−2244.

(11) Ivankin, A.; Henley, R. Y.; Larkin, J.; Carson, S.; Toscano, M. L.; Wanunu, M. *ACS Nano* **2014**, *8* (10), 10774−10781.

(12) Anderson, B. N.; Assad, O. N.; Gilboa, T.; Squires, A. H.; Bar, D.; Meller, A. *ACS Nano* **2014**, *8* (11), 11836−11845.

(13) Chansin, G. A.; Mulero, R.; Hong, J.; Kim, M. J.; DeMello, A. J.; Edel, J. B. *Nano Lett.* **2007**, *7* (9), 2901−6.

(14) Deshpande, S. V.; Gulari, E.; Brown, S. W.; Rand, S. C. *J. Appl. Phys.* **1995**, *77* (12), 6534−6541.

(15) Kim, B.-H.; Cho, C.-H.; Kim, T.-W.; Park, N.-M.; Sung, G. Y.; Park, S.-J. *Appl. Phys. Lett.* **2005**, *86* (9), 091908.

(16) Kim, T.-W.; Cho, C.-H.; Kim, B.-H.; Park, S.-J. *Appl. Phys. Lett.* **2006**, *88* (12), 123102.

(17) Park, N.-M.; Choi, C.-J.; Seong, T.-Y.; Park, S.-J. *Phys. Rev. Lett.* **2001**, *86* (7), 1355−1357.

(18) Wang, M.; Li, D.; Yuan, Z.; Yang, D.; Que, D. *Appl. Phys. Lett.* **2007**, *90* (13), 131903.

(19) Wang, Y. Q.; Wang, Y. G.; Cao, L.; Cao, Z. X. *Appl. Phys. Lett.* **2003**, *83* (17), 3474−3476.

(20) Larkin, J.; Foquet, M.; Turner, S. W.; Korlach, J.; Wanunu, M. *Nano Lett.* **2014**, *14* (10), 6023−6029.

(21) dela Torre, R.; Larkin, J.; Singer, A.; Meller, A. *Nanotechnology* **2012**, *23* (38), 385308.

(22) Sawafta, F.; Clancy, B.; Carlsen, A. T.; Huber, M.; Hall, A. R. *Nanoscale* **2014**, *6* (12), 6991−6996.
(23) Joo, C.; Balci, H.; Ishitsuka, Y.; Buranachai, C.; Ha, T. *Annu. Rev. Biochem.* **2008**, *77* (1), 51−76.
(24) Di Fiori, N.; Squires, A.; Bar, D.; Gilboa, T.; Moustakas, T. D.; Meller, A. *Nat. Nanotechnol.* **2013**, *8* (12), 946−951.
(25) Howitt, D. G.; Chen, S. J.; Gierhart, B. C.; Smith, R. L.; Collins, S. D. *J. Appl. Phys.* **2008**, *103* (2), 024310.
(26) Li, J.; Stein, D.; McMullan, C.; Branton, D.; Aziz, M. J.; Golovchenko, J. A. *Nature* **2001**, *412* (6843), 166−169.
(27) Huang, R.; Chen, K.; Han, P.; Dong, H.; Wang, X.; Chen, D.; Li, W.; Xu, J.; Ma, Z.; Huang, X. *Appl. Phys. Lett.* **2007**, *90* (9), 093515.
(28) Huang, R.; Chen, K.; Qian, B.; Chen, S.; Li, W.; Xu, J.; Ma, Z.; Huang, X. *Appl. Phys. Lett.* **2006**, *89* (22), 221120.
(29) McNally, B.; Wanunu, M.; Meller, A. *Nano Lett.* **2008**, *8* (10), 3418−22.
(30) Kim, H. M.; Lee, M. H.; Kim, K. B. *Nanotechnology* **2011**, *22* (27), 275303.
(31) Storm, A. J.; Chen, J. H.; Ling, X. S.; Zandbergen, H. W.; Dekker, C. *Nat. Mater.* **2003**, *2* (8), 537−540.
(32) Zheng, H.; Liu, Y.; Cao, F.; Wu, S.; Jia, S.; Cao, A.; Zhao, D.; Wang, J. *Sci. Rep.* **2013**, *3* (1920), 1−5.
(33) Kim, M. J.; Wanunu, M.; Bell, D. C.; Meller, A. *Adv. Mater.* **2006**, *18* (23), 3149−3153.
(34) Kistner, J.; Chen, X.; Weng, Y.; Strunk, H. P.; Schubert, M. B.; Werner, J. H. *J. Appl. Phys.* **2011**, *110* (2), 023520.
(35) Boulitrop, F.; Dunstan, D. J. *Phys. Rev. B* **1983**, *28* (10), 5923−5929.
(36) Mo, C. m.; Zhang, L.; Xie, C.; Wang, T. *J. Appl. Phys.* **1993**, *73* (10), 5185−5188.
(37) Dal Negro, L.; Yi, J. H.; Michel, J.; Kimerling, L. C.; Chang, T.-W. F.; Sukhovatkin, V.; Sargent, E. H. *Appl. Phys. Lett.* **2006**, *88* (23), 233109.
(38) Yokota, T.; Murayama, M.; Howe, J. M. *Phys. Rev. Lett.* **2003**, *91* (26), 265504.